Improvement of Light Load Efficiency for Buck-Boost DC-DC converter with ZVS using Switched Auxiliary Inductors

Hayato Higa
Dept. of Energy Environment Science Engineering
Nagaoka University of Technology
Nagaoka, Niigata, Japan
hhiga@stn.nagaokaut.ac.jp

Akira Sagawa
Dept. of Electric Information Engineering
Nagaoka University of Technology
Nagaoka, Niigata, Japan
sagawa_electro@stn.nagaokaut.ac.jp

Jun-ichi Itoh
Dept. of Electric Engineering
Nagaoka University of Technology
Nagaoka, Niigata, Japan
itoh@vos.nagaokaut.ac.jp

***Abstract*—This paper proposes a changing buck-boost inductance for non-isolated bidirectional buck-boost DC-DC converter with zero voltage switching (ZVS) modulation in order to achieve high efficiency at wide load region and a wide voltage variation. In the proposed converter, the auxiliary inductor and the bidirectional switch are connected in parallel to a main inductor, and each connection is switched depending on the load condition. At the light load region, the bi-directional switch is turned off for the reduction of the converter loss with the large equivalent inductance. On the other hands, the auxiliary circuit is utilized at the heavy load region in order to extend the power translation range with the small equivalent inductance. In addition, the sequence for the switching auxiliary inductor is also proposed in order to prevent the surge voltage of the bidirectional switch and the DC offset current in the auxiliary inductor. From the experimental results, the root mean square value of the inductor current is reduced by up to 23.8% compared with that of the conventional converter. In addition, the validity of the proposed sequence is also confirmed, e.g. no surge voltage at the turn off of the auxiliary inductor. Moreover, 41% of the converter loss reduction at the light load region.**

Keywords— Bidirectional DC-DC converter; Zero voltage switching; switching inductance

I. INTRODUCTION

Recently, energy storage systems (ESS) have been applied in DC micro-grid systems [1]-[3]. In ESS, a bidirectional buck-boost DC-DC converter is generally required to obtain the bidirectional operation regardless of DC-bus and battery voltage conditions. In a power converter for ESS, the power fluctuation due to renewable energy resources is compensated. In addition, the power oscillation can vary over a wide range of level, whereas the battery voltage in ESS fluctuates due to a charge and discharge operation. Hence, it is crucially required for ESS to be able to achieve the high efficiency in wide load range and under any condition of battery voltage variation [4]. However, the typical buck-boost converter topology with a continuous current mode is the low overall efficiency due to the switching loss of the hard switching operation [5].

In order to reduce the switching loss, the soft switching methods have been actively researched [6]-[8]. In the reference of [6], a zero voltage switching (ZVS) techniques which utilize a resonance between additional components and the junction capacitors have been proposed. In this method, the duty ratio range is limited by the resonance period. Besides, a zero voltage transient (ZVT) circuit is also proposed in order to achieve ZVS with entire load region by [7], [8]. By this method, the inductor current flow is controlled in order to discharge the junction capacitor of the switching devices. However, the additional conduction and the switching losses occur in ZVT circuit, i.e. the lower converter efficiency.

As different approaches, there are several modulation methods to achieve the soft switching [9-11], such as a triangular-current mode (TCM) applied for the achievement of ZVS [9], [10]. However, the converter efficiency at the light load becomes lower due to the high current ripple. Meanwhile, the control method to achieve ZVS for a four-switch-buck-boost DC-DC converter without additional components has been proposed [11]. In this method, the current ripple is reduced compared to that of TCM. However, the current ripple is still large in order to achieve ZVS over entire load. Furthermore, there is tradeoff between the current ripple and the high power capability. In other words, the problem in this method is low efficiency at the light load.

This paper proposes adding an auxiliary circuit with small inductors in order to achieve the high efficiency in wide load conditions including the high power capability. In particular, the bidirectional switches and the auxiliary inductors are connected parallel to the main inductor in order to reduce the current ripple at the light load. The originality of this paper is changing the equivalent inductance depending on the voltage variation and the load condition. Note that the current rating of the bi-directional switches and all inductors become small because the auxiliary inductors are connected in parallel to the main inductor. Moreover, sequence method for the switching auxiliary inductor is proposed to prevent the occurrence of DC-offset current in the auxiliary-inductor current. This paper is organized as follows; first, the circuit configuration and the operation modes with the ZVS achievement are explained. Second, the auxiliary circuit with the small inductors is introduced. Third, the proposed switching sequence is introduced. Finally, the effectiveness of the proposed circuit and sequence are confirmed by the experimental results.

II. CIRCUIT CONFIGURATION AND OPERATION PRINCIPLE

A. Circuit Configration

Figure 1 shows the circuit configuration of the four-switch buck-boost converter with the switched auxiliary small inductors. In order to minimize the inductors, the switching frequency is increased. This leads to the increase in the switching loss due to the higher switching frequency. In order

978-1-5386-6054-6/18/$31.00 ©2018 IEEE

to avoid this problem, the soft switching method is employed. In addition, the auxiliary inductors are changed in accordance with the output power.

B. Operation princeple

Figure 2 shows the bidirectional operation waveforms of the switching period with the ZVS achievement [10]. In both power flow operation, there are four modes in the switching period. In order to achieve ZVS, the offset of the inductor current I_0 is maintained during the zero-current interval of a conventional discontinuous current mode. The offset current for the ZVS achievement I0 is calculated by

$$I_0 = V_{in}\sqrt{\frac{C_{ds}}{L_{all}}}\,\frac{\sqrt{2}}{\sin\dfrac{T_d}{\sqrt{2C_{ds}L_{all}}}} \tag{1}$$

where C_{ds} is the junction capacitor of MOSFET, L_{all} is the total inductance including the main inductance L and the auxiliary inductors.

In addition, the transferred power is determined by the secondary voltage v_2 and the inductor current. Thus, the transferred power is calculated by

$$\begin{aligned} P &= \frac{1}{2\pi}\int_0^{2\pi} v_2(\theta) i_L(\theta) d\theta \\ &= \frac{V_{bus}}{4\pi\omega_{SW}L_{all}}\left[\begin{array}{l} 2V_{bat}\theta_1\theta_2 - 2\omega_{SW}L_{all}I_0\theta_1 \\ +V_{bus}\theta_2^2 - V_{bat}\theta_1^2 - V_{bat}\theta_2^2 \end{array}\right] \end{aligned} \tag{2}$$

Next, the each switching timing θ_1-θ_3 is calculated by (3)-(5).

$$\theta_1 = \frac{\omega_{SW}LI_0V_{bus} + V_{bat}^2\theta_3}{V_{bus}^2 + V_{bus}V_{bat} + V_{bat}^2} \tag{3}$$

$$\theta_2 = \frac{V_{bat}}{V_{bus}}(\theta_3 - \theta_1) \tag{4}$$

$$\begin{aligned} \theta_3 = &\frac{\omega_{SW}L_{all}I_0(V_{bus}+V_{bat})}{V_{bus}V_{bat}} \\ &+\sqrt{\left\{\frac{(\omega_{SW}LI_0)^2 + 4\pi\omega_{SW}L_{all}P_{ref}}{V_{bus}^2V_{bat}^2}\right\}\left(V_{bus}^2 + V_{bus}V_{bat} + V_{bat}^2\right)} \end{aligned} \tag{5}$$

where ω_{SW} is the switching angular frequency, P_{ref} is the reference transferred power.

It should be noted that the total inductance L_{all} is decided by the number of the auxiliary inductors. In the discharge operation, the switching timing of S1 and S3 are switched. At the condition of θ_3=2π, the maximum transferred power is achieved. The maximum average power P_{max} can be calculated by

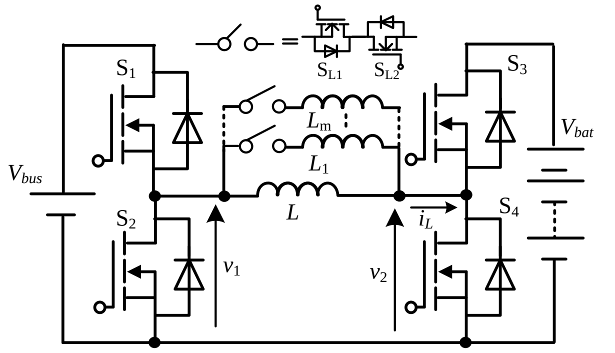

Fig. 1. Circuit configuration of bidirectional buck-boost converter with switched auxiliary inductors. The DC bus voltage varies from 300 V to 400 V, whereas the battery voltage changes from 300 V to 350 V.

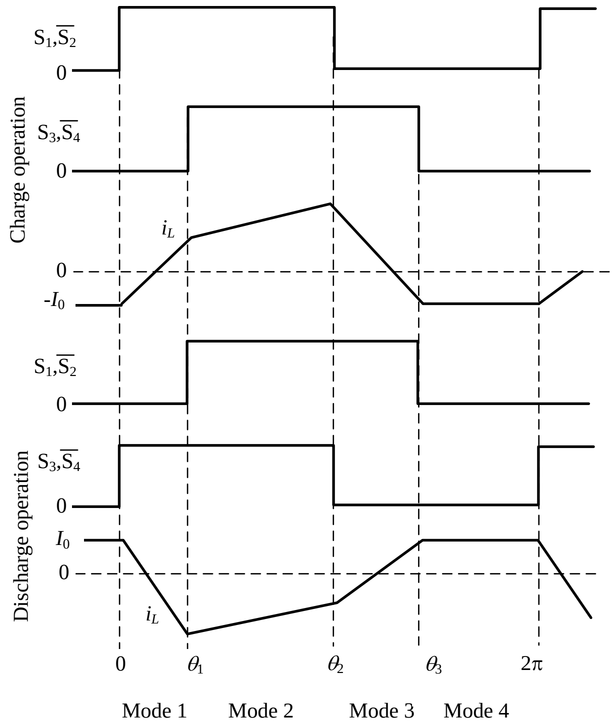

Fig. 2. Operation waveforms of switching period with ZVS achievement. In this method, the offset current I_0 is generated in order to satisfy ZVS condition. In the discharge operation, the switching timing of S_1 and S_3 are switched.

$$\begin{aligned} P_{\max} = &\frac{V_{bus}V_{bat}}{\left(V_{bus}^2 + V_{bus}V_{bat} + V_{bat}^2\right)} \\ &\left\{\frac{\omega_{SW}L_{all}}{4\pi}I_0^2 - I_0(V_{bus}+V_{bat}) + \frac{\pi V_{bus}V_{bat}}{\omega_{SW}L_{all}}\right\} \end{aligned} \tag{6}$$

As shown in (6), the maximum transferred power which can still achieve ZVS can be increased when the inductor value becomes small.

Figure 3 shows the inductor current waveforms at the light load condition. With the large inductance, the peak current can be reduced at the light load compared to that of the small inductor value. In addition, the offset current for ZVS I_0 is also reduced by increasing inductance from (1). Figure 4 shows the root mean square (RMS) current of the inductor current. RMS value of the inductor current is reduced by the large inductance. The problem with only one main inductor is that the maximum power becomes small when the inductance is large. In the conditions of the low inductance, the current ripple at the light load increases, i.e. the lower efficiency at the light load. In order to solve this tradeoff relationship between the power capability and the light load efficiency, the inductance is changed in accordance with the transferred power.

Figure 4 shows the root mean square (RMS) current of the inductor current. RMS value of the inductor current is reduced by the large inductance. The problem with only one main inductor is that the maximum power becomes small when the inductance is large. In the conditions of the low inductance, the current ripple at the light load increases, i.e. the lower efficiency at the light load. In order to solve this tradeoff relationship between the power capability and the light load efficiency, the inductance is changed in accordance with the transferred power.

III. SWITCHING SEQUENCE OF AUXILIARY INDUCTOR

At the switching auxiliary inductor, the DC offset current might occur at the turn-on timing of the auxiliary switches. Furthermore, the surge voltage occurs in accordance with the turn-off timing of the auxiliary inductor. In order to prevent the occurrence of the surge voltage and the DC-offset current, the following switching sequence is proposed.

Figure 5 shows the switching sequence for the switching auxiliary inductor. Fig. 5 (a) and (b) show the turn-on and the

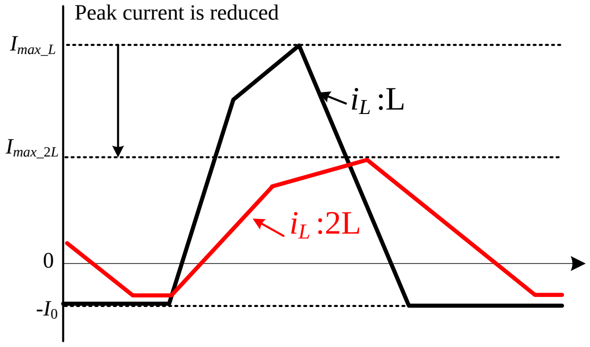

Fig. 3. Inductor current waveforms at light load when the inductance is changed. The peak current and RMS value are reduced by increasing the inductance.

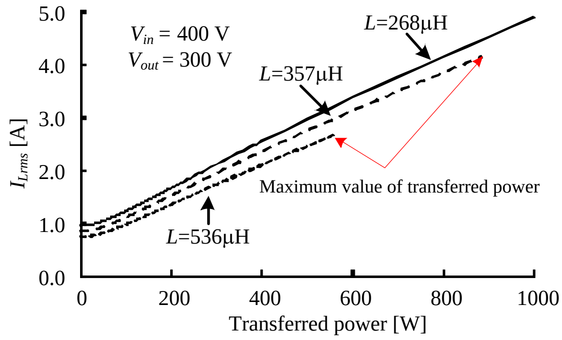

Fig. 4. RMS value of inductor current. At the light load, RMS value is reduced in proportion of the inductance. The larger inductance leads to the smaller transferred power. Therefore, the inductor value is changed by switching the auxiliary inductors.

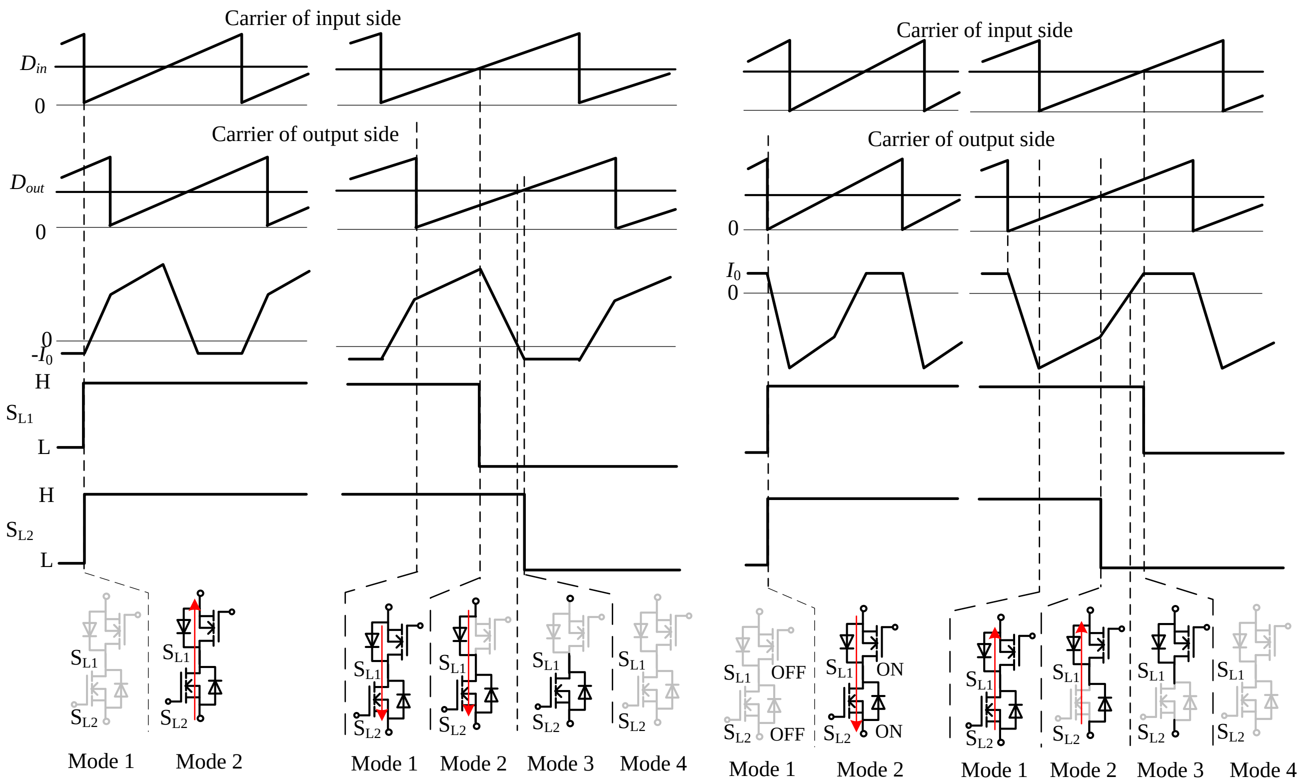

(a) Turn on at discharge operation (b) Turn off at charge operation (c) Turn on at discharge operation (d) Turn off at discharge operation
Fig. 5. In the proposed switching sequence, the current detection is not required because the switching timing is synchronized to the switching pattern of S_1 to S_4.

turn-off sequence at the charge operation, whereas Fig. 5 (c) and (d) show that at the discharge operation. In Fig. 5 (a) and (c), there is only one mode at the turn on of the bidirectional switch because the offset current is smaller than at the switching timing of S_1 and S_3. In Fig. 5 (b) and (d), there are four modes in the turn off of the auxiliary switches. In the Mode 1 of the charge operation, S_{L1} and S_{L2} are on at the input-side carrier peak, whereas S_{L1} and S_{L2} are on at the output-side carrier peak. In the mode 1 of Fig. 5 (b), S_{L1} and S_{L2} are on.

IV. EXPERIMENTAL RESULTS

A. *Experimental conditions*

A 1.0-kW prototype is tested in order to evaluate the proposed buck-boost converter with the switched auxiliary inductor. Table I shows the experimental parameters. At the both legs, IRFP460 (VISHAY) is selected. IRFP460 (VISHAY) has the on-state resistance R_{on} = 270 mΩ, the voltage rating V_{rate} = 500 V and the current rating I_{rate} = 20 A. Note that the minimum current for ZVS I_0 is calculated with about two times margin.

B. *Steady state operation*

Figure 6 shows the operation waveforms at the charge operation. It should be noted that the experimental conditions are the input voltage of 300 V and the output voltage of 350 V. Fig. 6 (a) shows that with auxiliary inductor, whereas Fig. 6 (b) shows that without auxiliary inductor. By applying the modulation for the ZVS achievement, the inductor current at the switching timing is also larger than the minimum current I0 at light load, i.e. ZVS achievement. In Fig. 6 (b), the minimum current for ZVS is reduced by the large inductance. In Fig. 6, the RMS value with the auxiliary inductor is reduced by 23.8% compared to that without the auxiliary inductor at the same load.

Figure 7 shows the operation waveforms at the discharge operation. Fig. 7 (a) shows that with the auxiliary inductor, whereas Fig. 7 (b) shows that without the auxiliary inductor. It should be noted that the experimental conditions are the input voltage of 300 V and the output voltage of 350 V. In Fig. 7, the current direction is difference from Fig. 5, i.e. the changing the power flow. By applying the modulation for the ZVS achievement, the inductor current at the switching timing is also larger than the minimum current I_0 at the light load. By applying the switching auxiliary inductor, the inductor current is reduced by 23.8%. In Fig. 7 (b), the minimum current for ZVS I_0 is also reduced by the large inductor value. The RMS value with the auxiliary inductor is reduced by 18.2%.

C. *Transient Response at Switching Axiliary Inductor*

Figure 8 shows the transient waveforms of switching auxiliary inductor at the discharge operation. In Fig. 8(a), the auxiliary inductor current is flown after the turn on of the auxiliary switch. In addition, it is confirmed that the DC offset of the auxiliary-inductor current is only the offset current for ZVS I_0. In Fig. 8(b), the auxiliary inductor current has been flown after the turn off of S_{L1}. Then, S_{L2} is turned-off when the auxiliary-inductor current becomes zero. Thus, the surge voltage does not occur because the body diode of S_{L1} is turned off naturally. Therefore, the low voltage rating device can be selected by applying the proposed switching sequence.

Figure 9 shows the transient waveforms of switching the auxiliary inductor at the discharge operation. Fig. 9 (a) shows

Table II Experimental conditions

Element	Symbol	Value
Rated power	P_{rated}	1.0 kW
DC-bus voltage	V_{bus}	400 V, 300 V
Battery voltage	V_{bat}	300 V, 350 V
Dead time at HV side	T_d	1 μs
Main inductor	L	532 μH
Auxiliary inductor	L_1	532 μH
Swiching frequency	f_{sw}	50 kHz
Minimum current with L_1	I_0	1.5 A
Minimum current w/o L_1	I_0	1.7 A
MOSFET		IRFP460 (VISHAY) V_{rate}=500 V, I_{rate}=20 A, R_{on}=0.27 Ω

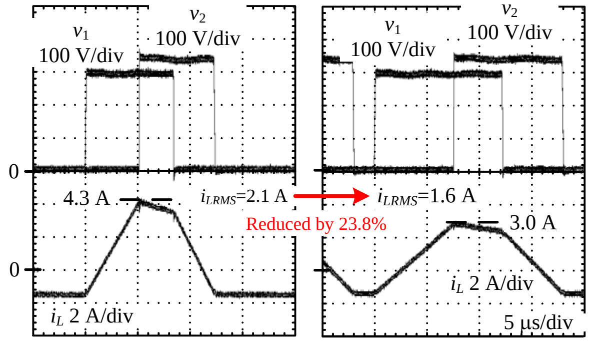

(a) With L_{aux} (b) Without L_{aux}

Fig. 6. Operation waveforms at charge operation. Without the auxiliary inductor, RMS value of the inductor current is reduced by 28.6% compared with the auxiliary inductor.

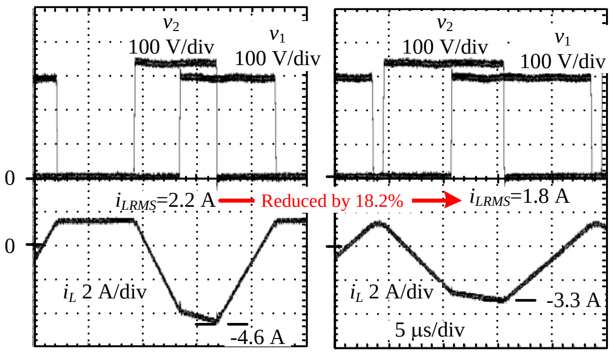

(a) With L_{aux} (b) Without L_{aux}

Fig. 7. Operation waveforms at discharge charge operation. In Fig. 7, the discharge operation is achieved because the direction of the inductor current is changed. Without the auxiliary inductor, RMS value of the inductor current is reduced by 28.6% compared with the auxiliary inductor.

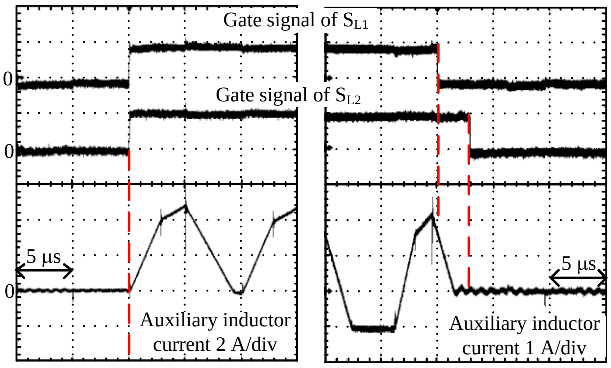

(a) Turn on of L_{aux} (b) Turn off of L_{aux}

Fig. 8. Transient waveforms of switching auxiliary inductor L_{aux} at charge operation. In Fig. 8 (a), the DC offset current is only the offset current for ZVS I_0.

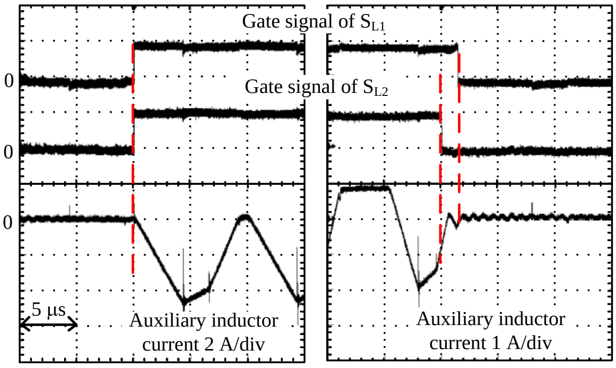

(a) Turn off of L_{aux} (b) Turn off of L_{aux}

Fig. 9. Transient waveforms of switching auxiliary inductor L_{aux} at discharge operation. In Fig. 9 (a), the DC offset current is only the offset current for ZVS I_0.

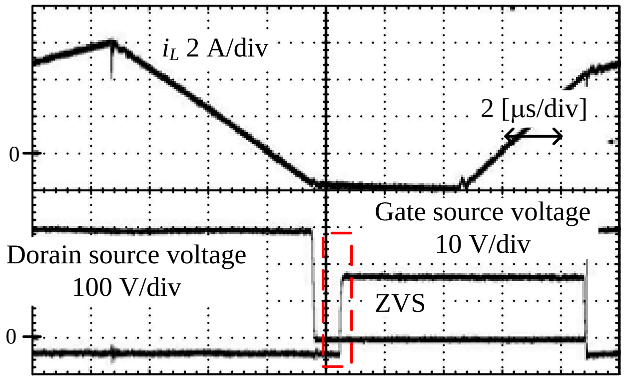

(a) S_1

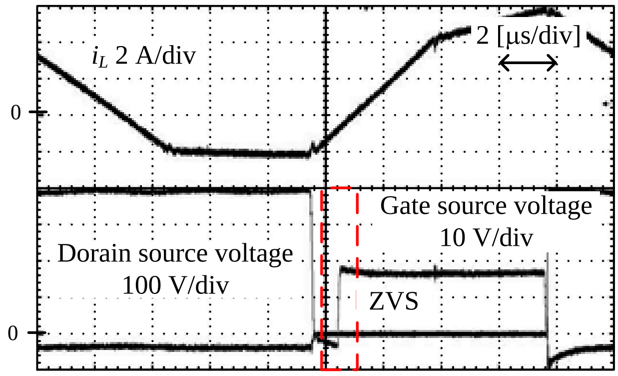

(b) S_4

Fig. 10. Operation waveforms of gate signal and drain-source voltage. In Fig. 10 (a) and (b), ZVS is achieved by the offset current for ZVS. In addition, the turn-off loss can be reduced by connecting a snubber capacitor in parallel to the main switches.

that at the turn on of the bidirectional switch, whereas Fig. 9(b) shows that at the turn off of the bidirectional switch. In Fig. 9(a) and (b), it is also confirmed that the DC offset of the auxiliary-inductor current is only the offset current for ZVS I_0. In addition, the auxiliary inductor current has been flown after the turn off of S_{L1}. Then, S_{L2} is turned-off when the bidirectional inductor current becomes zero. Thus, the surge voltage does not occur because the body diode of S_{L1} is turned off naturally.

D. ZVS operation

Figure 10 shows the operation waveforms of the gate signal and the drain-source voltage. Fig. 10 (a) shows the operation waveforms of S1, whereas Fig. 10 (b) shows that of S4. In Fig. 8, ZVS is achieved because the main switch is turned on at zero voltage. In addition, the surge voltage does not occur due to no recovery current at the both legs. In addition, the turn off loss can be reduced by connecting a snubber capacitor in parallel to the main switches.

E. Efficiency characteristics

Figure 11 shows the efficiency characteristics with/without the auxiliary inductor at the bidirectional operation. Fig. 11 (a) shows the efficiency characteristics at the input voltage of 400 V and the output voltage of 300 V, whereas Fig. 11 (b) shows the efficiency characteristics at the input voltage of 300 V and the output voltage of 350 V. In Fig. 11, the converter efficiency at the light-load range is improved by the large inductance. In other words, the converter loss is reduced by up to 41%. In addition, the maximum efficiency of 98.7% is achieved as shown in Fig. 11 (a) of the light load. By changing the auxiliary inductor depending on the transferred power, the high power capability is obtained. At the rated power, the converter efficiency is 98.3% at the rated power. Moreover, the high efficiency over the wide load range is achieved.

F. Load step response

Figure 12 shows the transient waveforms at the step-up load and the step-down load. Fig. 12 (a) shows the step-up load from 300 W to 500 W, whereas Fig. 12 (b) shows the step-down load from 500 W to 300 W. In Fig. 12, the stable current response is confirmed. In addition, the minimum current for ZVS is still achieved the both step-up and the step-down load, i.e. achievement of ZVS at the transient response of the step-up and the step-down load.

V. CONCLUSION

This paper proposed the four-switch-buck-boost converter with the switched auxiliary inductor in order to improve the light load efficiency and achieve the high power capacity. In the modulation method of the buck-boost converter, the inductor current including the offset current was applied in order to achieve ZVS. In the proposed circuit, the auxiliary inductors were switched in accordance with the transferred power and the voltage conditions. By switching the auxiliary inductor, the converter losses at light load was reduced. In addition, the switching sequence for auxiliary inductor was proposed. In the experiment, the validity of the proposed

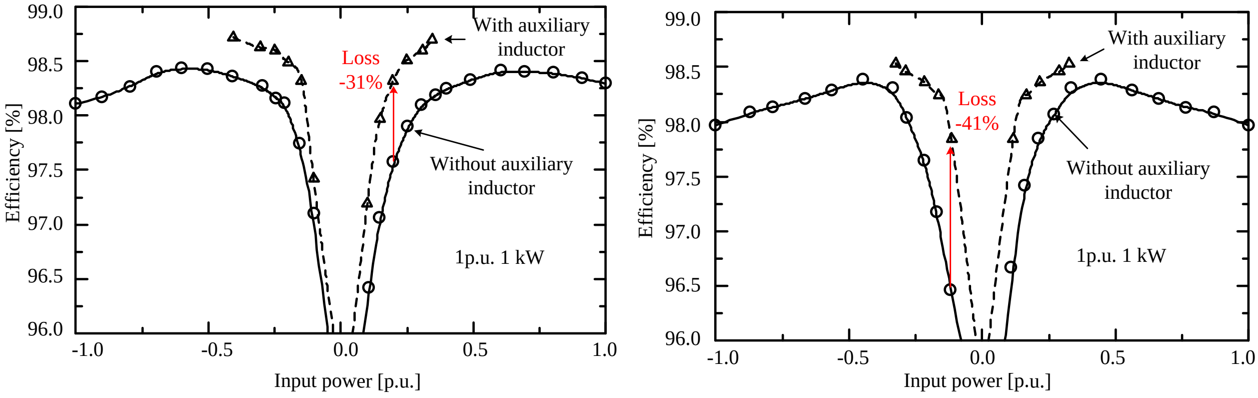

(a) V_{in}=400V, V_{out}=300V (b) V_{in}=300V, V_{out}=350V

Fig. 11. Efficiency characteristics with/without auxiliary inductor. By applying the large inductor value, the converter efficiency at the light load is improved. In addition, the high power capability is obtained when the auxiliary inductor is active.

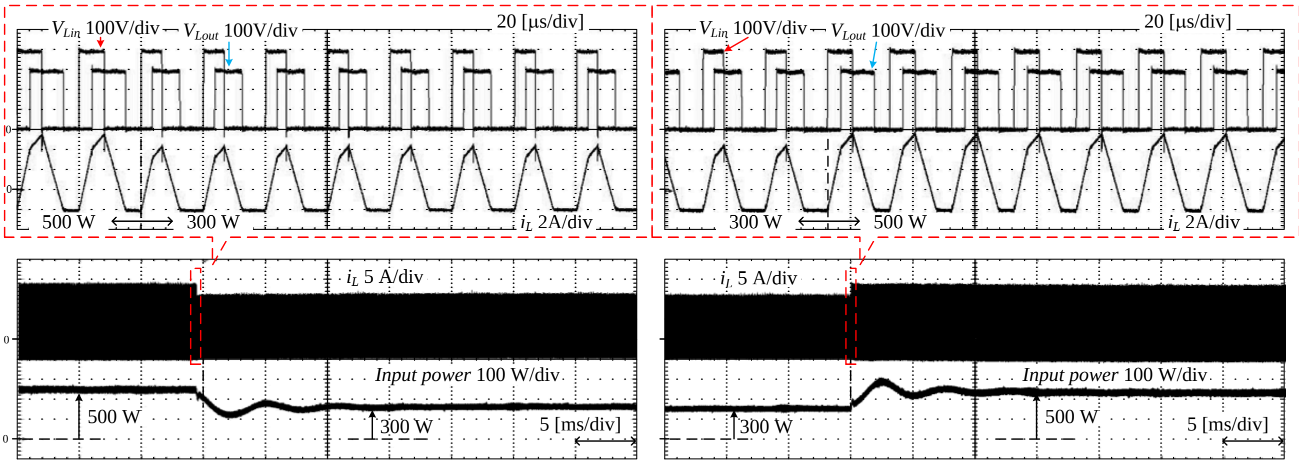

(a) Reference power change: 500 W to 300 W (b) Reference power change: 300 W to 500 W

Fig. 12. Transient waveforms at step-up load and step-down load. In Fig. 12, the inductor current is seamlessly changed at the step-up and the step-down load. In addition, the minimum current for ZVS is kept both the step-up and the step-down load.

method was confirmed by a 1.0-kW prototype. As results, RMS value of the inductor current was reduced by up to 23.8%. In other words, the converter loss at the light load was reduced by up to 41 % compared to that with the auxiliary inductor. Therefore, the high efficiency over wide load was achieved by switching the auxiliary inductor. In addition, the auxiliary inductor is smoothly changed by the proposed switching sequence. In future work, the design method for the auxiliary inductor will be considered.

References

[1] N. Hatziargyriou, H. Asano, R. Iravani, C. Marnay, "Microgrids", IEEE Power Energy Mag., Vol. 6, No. 3, pp. 78-94 2008

[2] H. Kakigano, Y. Miura, and T. Ise, "Low-Voltage Bipolar-Type DC Microgrid for Super High Quality Distribution," IEEE Trans. Power Electron., vol. 25, no. 12, pp. 3066-3075, 2010.

[3] T. Dragičević, X. Lu, J. C. Vasquez and J. M. Guerrero, "DC Microgrids—Part II: A Review of Power Architectures, Applications, and Standardization Issues," in IEEE Transactions on Power Electronics, vol. 31, no. 5, pp. 3528-3549, 2016.

[4] G. Lancel et al., "Energy storage systems (ESS) and microgrids in Brittany islands," in CIRED - Open Access Proceedings Journal, vol. 2017, no. 1, pp. 1741-1744, 10 2017.

[5] R. M. Schupbach and J. C. Balda, "Comparing DC–DC converters for power management in hybrid electric vehicles," in Proc. IEMDC, Jun. 2003, vol. 3, pp. 1369–1374

[6] In-Hwan Oh, "A soft-switching synchronous buck converter for Zero Voltage Switching (ZVS) in light and full load conditions," 2008 Twenty-Third Annual IEEE Applied Power Electronics Conference and Exposition, pp. 1460-1464. (2008)

[7] S. R. Lee, J. Y. Lee, W. S. JWung, Y. J. Park, C. Y. Won: "ZVT interleaved bi-directional low voltage DC-DC converter with switching frequency modulation for MHEV", ICEMS2017, pp. 1-7 (2017).

[8] T. Bang, J. W. Park: "Development of ZVT-PWM Buck Cascaded Buck-Boost PFC Converter of 2 kW with Widest Range of Input Voltage", IEEE Trans. IE. (2017) IEEE Early Access Articles

[9] C. Marxgut, F. Krismer, D. Bortis, J. W. Kolar, "Ultraflat Interleaved Triangular Current Mode (TCM) Single-Phase PFC Rectifier," IEEE Trans. PELS, vol. 29, no. 2, pp. 873-882, (2014).

[10] M. Kaufmann, A. Tüysüz and J. W. Kolar, "New optimum modulation of three-phase ZVS triangular current mode GaN inverter ensuring limited switching frequency variation," PEMD 2016, pp. 1-6. (2016)

[11] Stefan Waffler, Johann W. Kolar: "A Novel Low-Loss Modulation Strategy for High-Power Bidirectional Buck + Boost Converters", IEEE Trans. PELS., Vol. 24, No. 6, pp. 1589-1599 (2009)